Electronic State-Resolved Evaporation Dynamics of Gallium Molten Metal

by Isehaq (Isaac) Alhuseini

Committee Members:
David Nesbitt (PHYS), Thesis Advisor
Paul Beale (PHYS), Honors Council Representative
Jordy Bouwman (CHEM), Outside Reader

A thesis submitted in partial fulfillment
of the requirements for the
Degree of Bachelor of Arts with Honors
in Physics

University of Colorado
Boulder, Colorado
April 10, 2024

Abstract

The gas-liquid interface represents a fascinating, albeit challenging, environment essential to understanding a wide range of atmospheric, chemical, and biological processes. This paper focuses on a relatively simple model system: quantum state resolved evaporation of metal atoms from the gas-molten metal interface. In particular, we combine hot molten metal crucibles in high vacuum (10^{-8} Torr) with high sensitivity laser-induced fluorescence (LIF) obtained from atoms in an Nd:YAG pumped-frequency tripled dye laser/photomultiplier (PMT) detection system. Specifically, we probe both ground and spin-orbit excited Ga($^2P_{1/2}$ and $^2P_{3/2}$) atoms evaporating from molten Ga metal as a function of temperature. The signal intensities and spin-orbit ratios permit quantitative assessment of: i) the thermodynamics and ii) the equilibrium vs. non-equilibrium nature of the atomic evaporation event, respectively. The temperature dependence of the Ga signals permits rigorous extraction of vaporization enthalpies (ΔH_{vap}) for such ultralow vapor pressure molten metal systems. In this paper, we establish that the system shows non-equilibrium dynamics in the range 700-900C. Further investigation is needed for an observation of the dynamics with no oxide film on the liquid metal and at a wider temperature range.

Acknowledgment

I would like to thank Prof. David Nesbitt for his support and guidance throughout this project. I would also like to thank Mikhail Ryazanov for making this project happen through his support and day-to-day guidance.

Table of Contents

1. Introduction

The gas-liquid interface represents a fascinating albeit challenging environment essential to understanding a wide range of atmospheric, chemical, and biological processes. These processes are involved in breathing, distillation, and climate propagation. Studies have been conducted on complex gas-liquid systems including collision dynamics studies [1], and aqueous evaporation dynamics studies [2]. However, few studies have investigated the evaporation dynamics of molten metals, although many articles have proposed theoretical models for this system [4].

We aim to evaluate the equilibrium vs non-equilibrium dynamics for evaporated gallium Ga, e.g., whether an incident Ga ($^2P_{1/2}$ or $^2P_{3/2}$), atom approaching the molten metal "sticks" or "bounces" from the gas-liquid interface, using the means of LIF detection. We focus on this relatively simple model system: quantum state resolved

evaporation of metal atoms from the gas-molten metal interface. This simple system gives us an insight into the evaporation dynamics of various conductors that have yet to be studied at low temperature and density regimes. In particular, we use Laser Induced Fluorescence LIF signals to evaluate relative quantum state populations and assess the thermodynamics and behavior of the system at equilibrium. We use gallium as the subject of our studies as a metal that has an open shell ground state with a relatively small (826.19 cm^{-1}) spin-orbit splitting that makes the collection of high-resolution LIF signals possible. In addition, the relatively wide temperature range of liquid gallium (303 – 2676 K at standard pressure) allows us to explore a wide density range. More specifically, we first quantitatively evaluate the evaporation enthalpy ΔH_{vap} of the ground state and first spin-orbit excited Ga($^2P_{1/2}$ and $^2P_{3/2}$) atoms via Arrhenius plot using LIF signals. Our measurements are held at remarkably low densities, compared to previous measurements [3]. This novel method allows for measurements of vaporization enthalpy ΔH_{vap} at regimes that were out of experimental reach. Second, we evaluate the equilibrium vs. non-equilibrium nature of the atomic evaporation event using LIF signal intensity. We compare the measured intensity ratio to the predicted intensity ratio using the Boltzmann distribution characterized by the liquid temperature T_{liquid}. The experimental data agreeing with the Boltzmann distribution characterized by T_{liquid} would mean that the vapor is in thermal equilibrium with the liquid.

2. Background

2.1. Detailed Balance

To understand the equilibrium vs. non-equilibrium dynamics of evaporation at the gas-liquid interface, one must first look at the profound idea of detailed balance. The detailed balance principle follows from reversibility and classical thermodynamics. Detailed balance states that at equilibrium of some degree of freedom, the rates of each elementary process should be dependent on their reverse process rate [15]. The principle, thus, constrains the number of independent rate constants in the system. This tells us that for a system of gas in contact with a liquid surface, the rate of atoms leaving the surface must equal the rate of atoms being absorbed into the surface [4]. For example, looking at a system consisting of three different atoms [Figure 1], we can see that we have 6 rate constants going between those three atoms. However, detailed balance restricts the rate constants to only three independent rate constants.

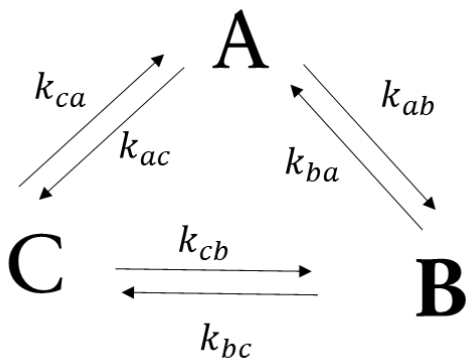

Fig. 1: A three atom system. k_{ij} is the rate constant of the process going from i to j. Note that at equilibrium, we only have three independent rate constants due to detailed balance.

In this study, we focus on the electronic state degree of freedom. We will probe the ground state and first spin-orbit excited state of gallium vapor to study whether the electronic state degree of freedom is in equilibrium when the system is in flux equilibrium or not, i.e. whether the detailed balance principle holds for the electronic degree of freedom in the gas-molten gallium interface or not. However, the translational degree of freedom is also relevant as the main goal of this study is measuring the electronic state-dependent flux through density measurements.

Using the detailed balance principle, we can see that all atoms that hit the liquid interface would get adsorbed and thermalized (stick), if the system is in macroscopic equilibrium. On the other hand, the system will not be in equilibrium if some atoms hitting the liquid surface "bounce" (i.e., inelastically scatter). If the probability of sticking/bouncing is dependent on the electronic state of the incoming atom, we will be able to measure that using the Boltzmann distribution.

2.2. Boltzmann Distribution

The Boltzmann distribution states that at equilibrium, the following is true for an energy state i:

$$P_i = g_i \frac{e^{-\varepsilon_i/kT}}{Q},$$

Where P_i is the population of the energy state, g_i is the degeneracy of the state, ε_i is the energy of the state, k is the Boltzmann constant, T is the temperature of the system,

and Q is the partition function of the system [12]. A two energy state system, then, could be characterized by the following formula:

$$\frac{P_i}{P_j} = \frac{g_i}{g_j} e^{-\Delta E/kT}, \qquad \Delta E = \varepsilon_i - \varepsilon_j.$$

To characterize the equilibrium vs. non-equilibrium dynamics, we will measure the population ratio of two quantum states leaving the liquid in vacuum and compare that to the population ratio calculated with the formula above characterized with the liquid temperature. If the measured ratio agrees with the calculated ratio, the probability of atoms bouncing off the liquid when incoming at the liquid-molten metal interface is close to zero – not measurable.

2.3. Arrhenius Behavior

To measure the heat of vaporization, we will use the Arrhenius equation. The Arrhenius equation states that

$$P_i \ \alpha \ e^{-E_a/kT},$$

$$\ln(P_i) = \frac{-E_a}{k}\frac{1}{T} + c,$$

Where P_i is the population of some state, E_a is the activation energy, T is the liquid temperature, and c is a constant [12]. When plotting the natural log of the population of the energy state vs. 1/T, the resulting plot will be a linear plot with the activation energy being -k*slope. The activation energy is an energy barrier the atoms need to overcome in order to leave the liquid. In our simple system, this activation energy is the heat of vaporization ΔH_{vap}.

2.4. Gallium Metal

Choosing a metal to study the evaporation dynamics of molten metal takes multiple considerations. The chosen metal should have relatively low melting temperatures (<500°C) to be able to melt using the resistive heating apparatus. This narrows down the candidate metals to low melting temperature metals such as mercury, gallium, and indium. The other requirement is having an open shell electron configuration promoting a spin-orbit splitting of $< 2000\ cm^{-1}$. Gallium metal satisfies those requirements with 29.8°C melting temperature and $826.19\ cm^{-1}$ splitting between the ground state ($^2P_{1/2}$) and the first spin-orbit excited state ($^2P_{3/2}$). The electronic configuration of gallium is [Ar] $3d^{10}\ 4s^2\ 4p^1$. The atomic spin is ½ (from the lone electron in the 4p subshell) and the open shell electron has orbital angular momentum = 1. This means that the possibilities for angular momentum j are j = 1/2 and j = 3/2.

3. Experimental Apparatus

We combine hot molten metal crucibles in high vacuum (10^{-8} Torr) with high sensitivity laser-induced fluorescence (LIF) obtained from atoms in an Nd:YAG pumped-frequency tripled dye laser/photomultiplier (PMT) detection system. Specifically, we probe both grounds and spin-orbit excited Ga($^2P_{1/2}$ and $^2P_{3/2}$) atoms evaporating from molten Ga metal as a function of temperature (600-1100K), for which the signal intensities and spin-orbit ratios permit quantitative assessment of i) the thermodynamics and ii) equilibrium vs. non-equilibrium nature of the atomic evaporation event, respectively. The temperature dependence of the Ga signals permits rigorous extraction

of vaporization enthalpies (ΔH_{vap}) for such ultralow vapor pressure molten metal systems. Conversely from time reversal symmetry and detailed balance considerations, the equilibrium vs. non-equilibrium spin orbit quantum state distributions report on the adsorption/desorption dynamics, e.g, whether an incident Ga ($^2P_{1/2}$ or $^2P_{3/2}$), atom approaching the molten metal "sticks" (i.e., adsorbs and thermalizes) or "bounces" (i.e., inelastically scatters) from the gas- liquid interface.

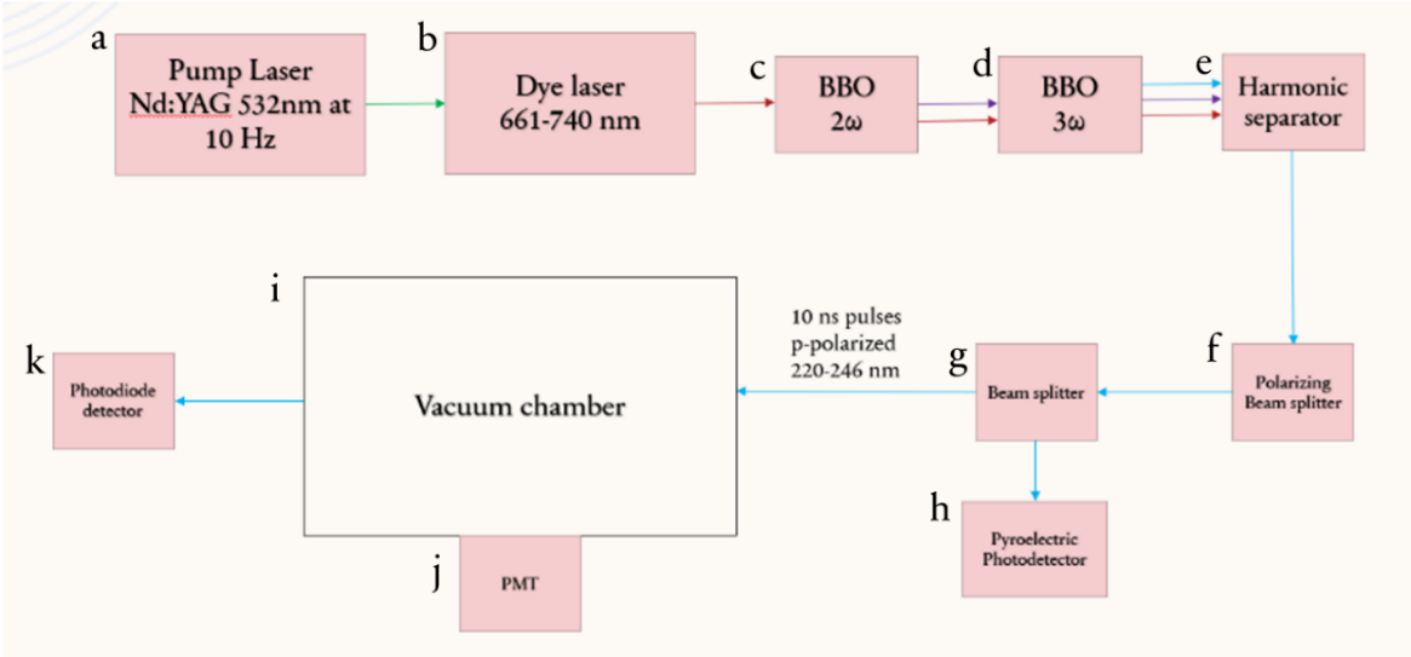

Fig. 2: The optical layout.

3.1. Pump Laser

The laser optical layout of the experiment (Fig.2) starts with a 10 Hz pulsed, Q-switched Nd:YAG laser (Fig.2.a) that has a fundamental wavelength $\lambda = 1064$ nm, with

pulse duration around 10 ns. The laser goes through second harmonic generation which outputs $\lambda = 532$ nm that will be used to pump the dye laser (Fig.2.b). The laser's pumping medium is neodymium-doped yttrium aluminum garnet (Nd:YAG) crystal that is pumped by flashlamps typically at 1.2kV [1,5].

The Nd:YAG laser utilizes active Q-switching technique using Pockels cell. The Quality Factor (Q factor) is a measure of the quality of the resonance of the optical cavity. The higher the Q factor, the narrower the bandwidth, the lower the Q factor, the wider the bandwidth [7]. Q-switching is a technique where the process starts by keeping the resonator at a high loss level to accumulate the energy in the gain medium to get to a population inversion state. After a certain time, the loss is switched to a low level suddenly; leading to simulated emission being probable and lasing happens [6, 8]. Q-switching is used to produce nanoseconds laser pulses with high energy [6]. Active Q-switching uses an active control element to manipulate the Q factor in the optical cavity. In our optical system, we use Powerlite Precision 8000 Nd:YAG laser to pump the dye laser at the required frequency. This laser uses a Pockels cell (Fig. 3. Component 5) to manipulate the polarity of the light and, consequently, the resonator loss level. The Pockels cell has a longitudinal field KD*P crystal that acts as a quarter wave plate when a high voltage (~ 3.6kV) is applied [5].

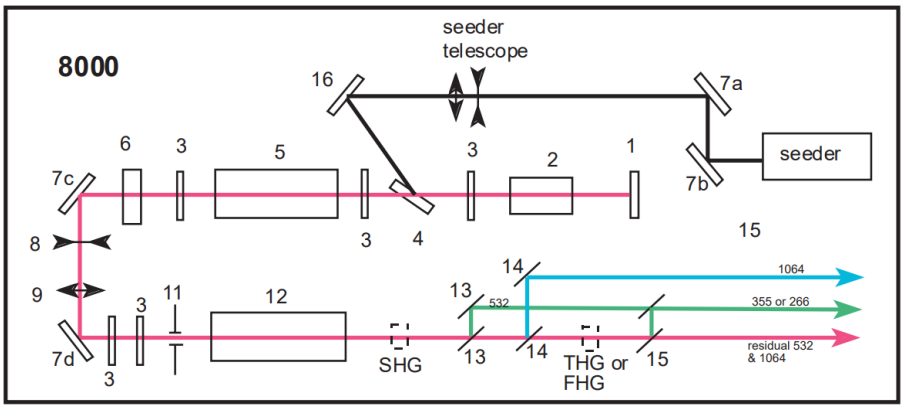

Fig. 3: Schematic of the Nd:YAG laser from laser manual [5]. 1.Mirror, 2. Pockels cell, 3. λ/4 plate, 4. Dielectric polarizer, 5. Flashlamp, 6. Output coupler, 7. Mirror, 8. Div. lens, 9. Con. Lens, 11. Pinhole, 12. Flashlamp, 13. 13. Dichroics, 532nm, 14. Dichroics, 1064nm, 15. Dichroics. 355nm or 266nm, 16. Mirror [5].

Figure 4 demonstrates the operation configuration of an open and closed cavity. When the Pockels cell is at 0 volts, the light gets rejected by the polarizer as it is vertical. This means high loss value in the cavity leading to a population inversion in the gain medium. However, when the Pockels cell is operating, the light beam passes through the polarizer resulting in an open cavity and lasing as simulated emission is probable with the feedback coming in.

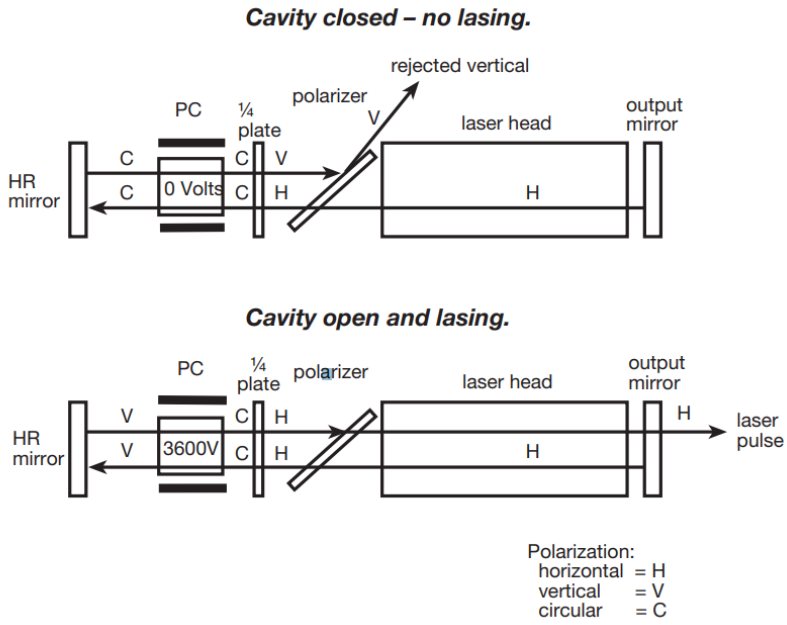

Fig. 3: demonstration of a closed cavity (Pockels cell at 0kV) and an open cavity (Pockels cell at 3.6kV) [5].

The laser has a fundamental frequency of 1064nm. The laser goes through second harmonic generation using a nonlinear beta barium borate crystal (BBO) resulting in 532nm laser beam that is used to pump the dye laser.

We mentioned earlier that Q-switching produces short laser pulses about 10ns for our system). This is intended to excite the evaporated atoms in the vacuum chamber without saturating the transition, i.e., keep pumping energy at already-excited atoms. To make sure that the transitions are not saturated, we need to looks at the lifetime of the upper quantum state of the transitions in consideration. We will study the gallium transitions from the ground state and first spin-orbit excited state ($^2P_{1/2}$ and $^2P_{3/2}$) with the upper state $4s^2 8s,\ ^2S_{1/2}$. The two transitions have lifetime of 317ns for the transition from the

ground state and 180ns for the transition from the spin-orbit excited state. The 10ns duration ensures no saturation of the transition occurs, giving us LIF signal that is in a linear regime.

3.2. Dye Laser

The Nd:YAG laser pumps the dye laser at 532nm. The laser used in our system is Continuum ND6000 Dye laser. The dye used is LDS 698, which operates with an oscillator and two amplifier cells in the range 661-740nm. This dye laser has a relatively small linewidth of $> 0.1\ cm^{-1}$ which ensures high-resolution LIF scanning [9]. Optimal concentrations of the dye in methanol were found to be 110mg/L for the oscillator and 40 mg/L for the amplifier. A 25,000 steps/turn stepped motor is used to move a translational stage, changing the angle of a turning mirror which controls the wavelength of the laser [9]. The motor uses the sine drive principle where linear translation of the stage translates to a linear change in wavelength [1]. A LabView program is used to scan the laser with a typical scanning speed of $0.5 - 0.2\ cm^{-1}/s$. The typical output energy of the dye laser is about 10 μJ/pulse.

Nonlinear crystals (BBO) (Fig.2.c&d) are then used to double and triple the light frequency via second and third harmonic generation. The first crystal combines two incoming photons using second harmonic generation to produce a frequency doubled laser pulse. The second BBO crystal combines the fundamental and doubled light via sum harmonic generation to produce frequency tripled light. Both crystals reside inside autotrackers (Inrad Autotracker III) that ensure optimum frequency doubling and tripling via active feedback mechanism [1]. The three frequencies are separated via a series of

prisms (Fig.2.e); the frequency tripled light is used, and the rest is discarded. A polarizing beam splitter on a rotating mount (Fig.2.f) is used to control the energy of the laser with maximum reflectivity of ~ 90%. Part of the beam is then picked up via another beam splitter (Fig.2.g) (9% transmitted to chamber) to measure the pulse-to-pulse energy of the beam on a pyroelectric photodetector (Fig.2.h). A typical working energy is 0.5 nJ in the chamber. The beam goes through Brewster's Angle window into the chamber. The laser is picked up after the chamber with a photodiode detector (Fig.2.k) for fine relative pulse-to-pulse energy measurement. The two transitions we are measuring are at $44332\ cm^{-1}$ and $43506\ cm^{-1}$.

3.3. Vacuum Chamber

The vacuum chamber has a typical working pressure of $\sim 10^{-8}\ Torr$. This high vacuum is achieved with a two-stage roughing pump (Edwards E2M30) and a turbomolecular pump (Pferffer TPH 1801 U P) with working frequency of 525 Hz. The pressure inside the chamber is obtained via a vacuum ionization gauge (Varian 843).

We seek to exclude atom-atom and atom-molecule collisions from the system to measure the true relative population of two quantum states in the vapor. To achieve that, we need the mean free path of all species inside the chamber to be much smaller than the dimensions of the chamber. If we assume a pressure of $10^{-8}\ Torr$ and a temperature of 1000K inside the vacuum chamber, and assuming oxygen is 20% of air with kinetic diameter 346 pm and nitrogen is 78% of air with kinetic diameter 364 pm [10, 11], we can calculate the mean free path (l) of the air molecules as follows [12]:

$$l = \frac{k_B T}{\sqrt{2}\,\pi\, d^2 P}$$

$$l_{O_2} = 97{,}350\, m$$

$$l_{N_2} = 22550\, m$$

Which means that the collision between air molecules is very unprobeable inside the $(0.5m)^3$ vacuum chamber. It remains to look at the mean free path of gallium vapor atoms. The gallium vapor pressure is $\sim 3.4 \times 10^{-6}\, Torr$ [17] and radius ~130pm [18].

$$l_{Ga} = 100\, m$$

The gallium metal sample needs to be heated to get a sufficient vapor density for the LIF detection. We use a low voltage power supply (LV400, R.D. Mathis Company) to provide high current that goes through an alumna coated tungsten (W) boat. The typical current used is in the range of 0-100 A corresponding to room temperature – 1300K. A tungsten boat (Fig. 5) is chosen as the heating element due to tungsten's high resistivity ($0.00196 \times 10^{-8} \Omega$ m at 20 °C), high melting point (3422 °C), and robustness at high temperatures, allowing for high temperatures without the boat melting or deforming [13]. The tungsten boat is coated with alumina (aluminum oxide Al_2O_2) which is an electrical insulator with high thermal conductivity (30 W/m K at 100 °C) [13].

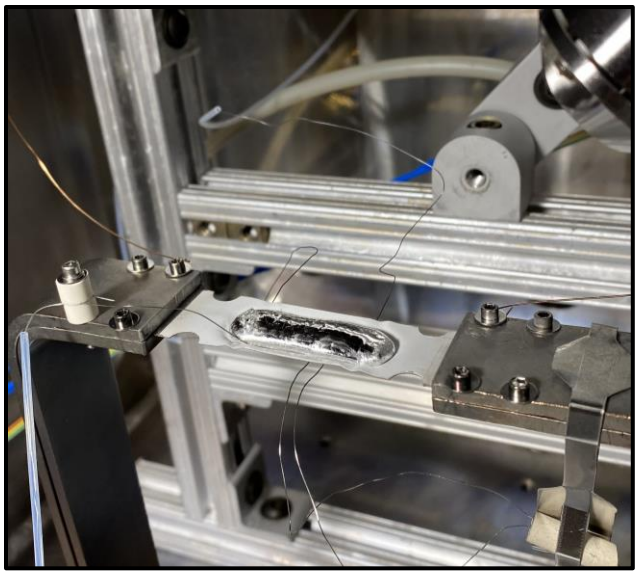

Fig. 5: A picture of the alumina coated tungsten boat inside the vacuum chamber with a gallium sample on the boat. A K-type thermocouple is welded to the bottom of the boat.

The gallium liquid temperature is measured via a K-type thermocouple that is laser-welded to the bottom center of the tungsten boat. The thermocouple has a standard limit of error of 0.75% (±6°C at 800°C). The thermocouple output is used in a feedback loop to control the current supply and stabilize the W boat tempurature.

The Laser-Induced Fluorescence (LIF) signal is obtained via a Photomultiplier Tube (PMT) (Fig.2.j) that is normal to the laser path. A photomultiplier tube (PMT) is a device that collects photons and convert them to an electrical current. When a photon hits the photomultiplier, it ejects an electron via the photoelectric effect. The electron then goes through an electron multiplier with high voltage (typically 1-1.8kV) to produce current [14]. The PMT signal is integrated over a 300 ns window with a boxcar integrator (SRS250). To avoid noise from scattered laser and induced emission, we start integrating the signal after the pulse duration.

3.4. Oxidation Considerations

Even at low pressure, a fractal oxide (Ga_2O_3) layer forms on top of gallium liquid with an estimated thickness of around 0.1μm (Figure 6) [16]. In addition to the thin film, larger oxide flakes accumulate as the experiment runs (Figure 7). To preserve the purity of the liquid gallium while taking measurements, the gallium oxidation must be cleaned and the oxidation must be slowed down. Previously used method to reduce the oxide film include Ar+ ion sputtering and mechanical exfoliation [1, 16, 19, 20].

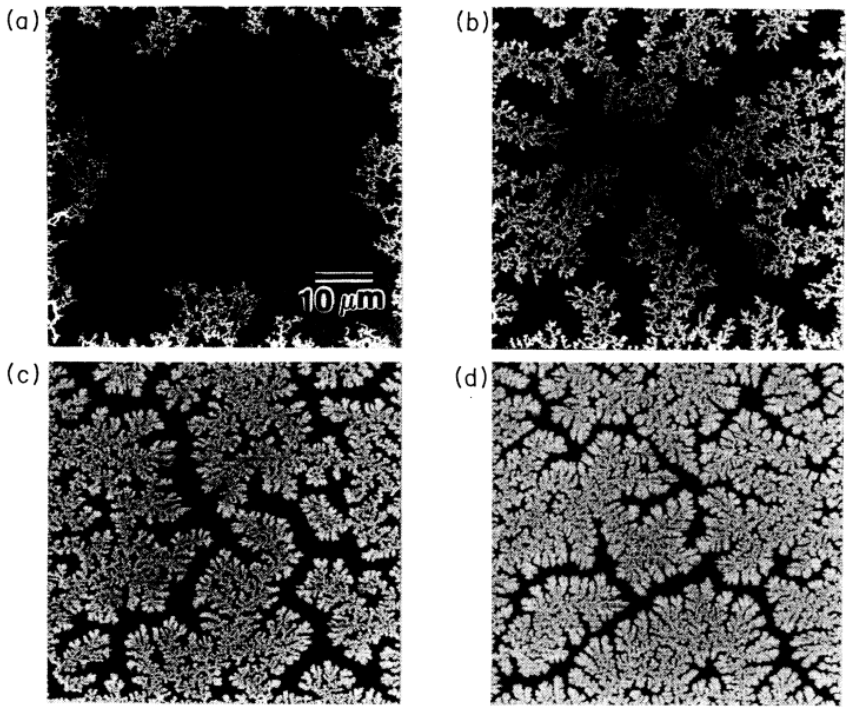

Fig. 6: gallium oxide growth across clean liquid gallium, imaged with SIMS signal at $P = 5 \times 10^{-7} Torr$ and $T = 27.7°C$. a) t = 60s, b) t = 300s, c) t = 1200s, d) t = 2400s.

Ion sputtering was tested with 2keV and $10^{-5}Torr$ argon leak [Figure 7]. The results show on noticeable effect on the ground state to spin-orbit excited state population ratio or improvement in the precision. Those results challenge the common practice of reducing the gallium oxide film using Ar+ ion sputtering.

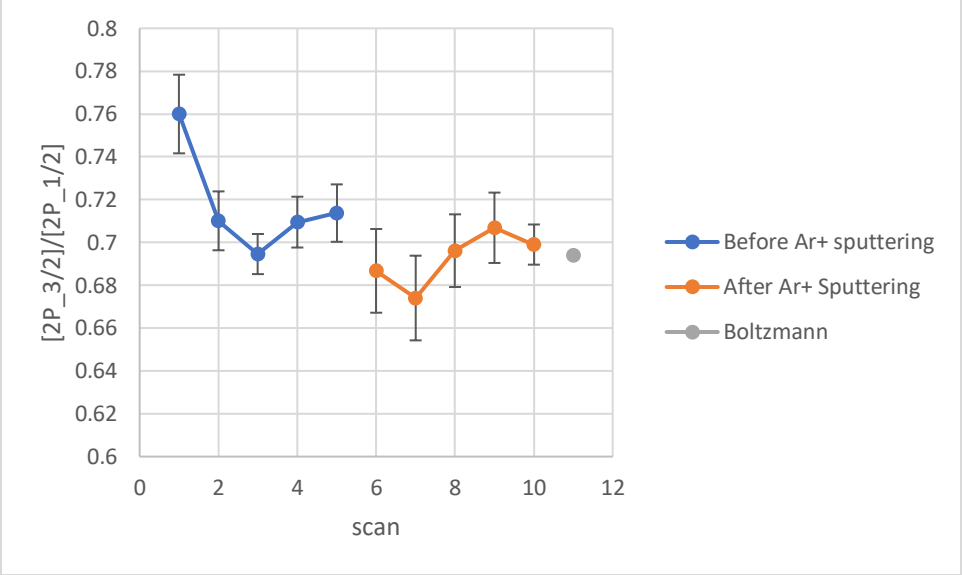

Fig. 7: The population ratio before and during the Ar+ ion sputtering. The last scan was taken two hours into the ion sputtering process. T = 850°C, $P = 2.5 \times 10^{-7}Torr$. Each ratio point is an average of 4 scans over an average of 4 scans.

Large flacks of gallium oxide could form when the experiment is being run for several days which typically need mechanical exfoliation to clean out. Large flacks of gallium oxide also move due to the apparatus small vibrations and surface tension of gallium liquid. This has been observed as in figure 8. A mechanical exfoliator is

suggested to minimize the need to open the vacuum chamber to clean the sample, as it would take about a day to get back to the previous base pressure.

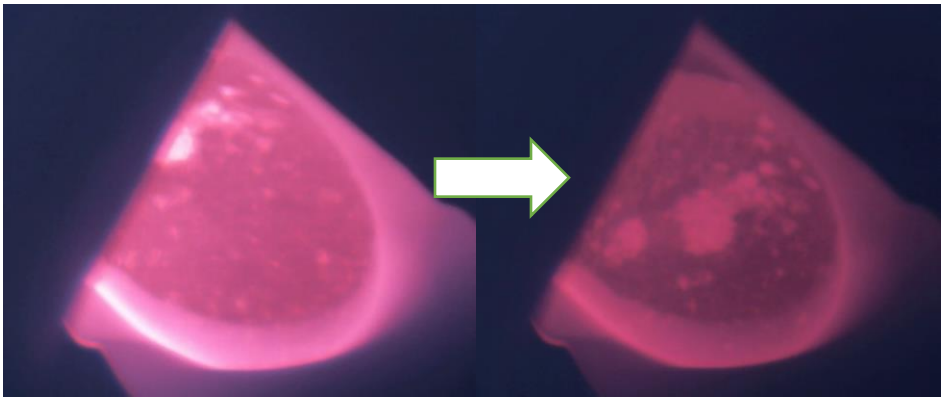

Fig. 8: pictures taken of the gallium sample at 850°C with a two hour duration between the two pictures.

4. Data Analysis

The LIF signal is normalized to the pulse-to-pulse laser energy. First, the photodiode (PD) signal is plotted against the pyroelectric photodetector (PEPD) signal using a linear fit with a zero y-intercept and a PD/PEPD constant ratio is obtained. The PMT signal is then normalized using the PD signal due to the high sensitivity of the PD to the pulse-to-pulse fluctuations. The PD/PEPD ratio is then used to modify the normalized PMT signal to be in the form PMT/PEPD instead of PMT/PD. This step allows us to compare different transitions to each other as the PD is sensitive to the wavenumber of the transition so it is more sufficient to look at the energy normalized signal PMT/PEPD instead of the intensity normalized signal PMT/PEPD.

The transition signal then goes through a base line subtraction obtained from a linear fit of points from the start and end of the scan. The resulting line is fitted with a two-gaussian function for practical reasons and parameters are calculated from this fit, including line amplitude, width, and integral. One of the gaussians is meant to fit the line wings while the other is meant to fit the peak (figure 9). Due to unresolved hyperfine structure, the two lines $^2P_{1/2}$ and $^2P_{3/2}$ have different widths, making it necessary to take the line the integral instead of amplitude as the quantity proportional to the line intensity. Figure 9 shows an example of the visual output of this process.

The line scans are typically taken in an algorithmic form to minimize the effect of the signal drifting over time due to oxidation of the gallium surface. For example, a typical data set is taken in the following order: 4 scans of the $^2P_{1/2}$ line followed by 4 scans of the $^2P_{3/2}$ line at each temperature, going up in temperature and then down through the same temperature set.

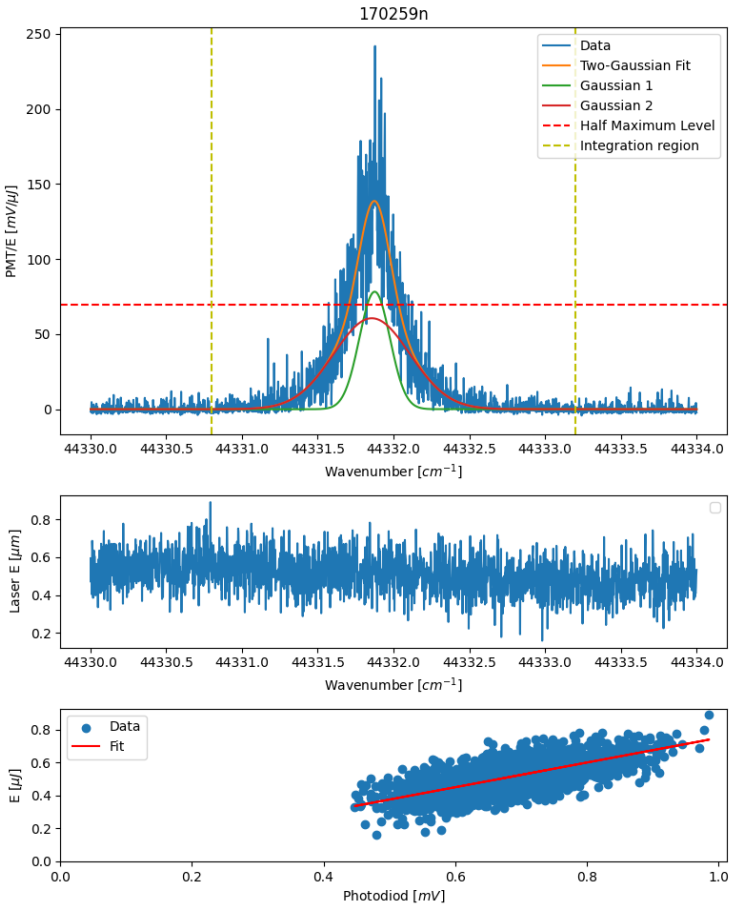

Fig. 9: The LIF signal of Ga ($^2P_{1/2}$) line at 750°C (top), the laser energy fluctuation as a function of wavenumber (middle), and the photodiode signal vs. the pyroelectric photodetector plot (bottom).

5. Results

Using the LIF data obtained, we can evaluate the thermodynamical heat of vaporization (vaporization enthalpy) for both the ground state and spin-orbit excited state at a wide temperature range. In addition, we can use the intensity ratio to study the equilibrium vs. non-equilibrium evaporation dynamics of gallium.

First, we evaluate the heat of vaporization using the Arrhenius relation,

$$\ln(I) = \frac{\Delta \mathrm{H_{vap}}}{k}\frac{1}{T} + constant.$$

where E_a is the activation energy corresponding to vaporization enthalpies ΔH_{vap} (the latent heat of vaporization) in our case. We obtain the Arrhenius plots (Figure 10) with the slope corresponding to the following relation:

$$Slope = \frac{\Delta \mathrm{H_{vap}}}{k}$$

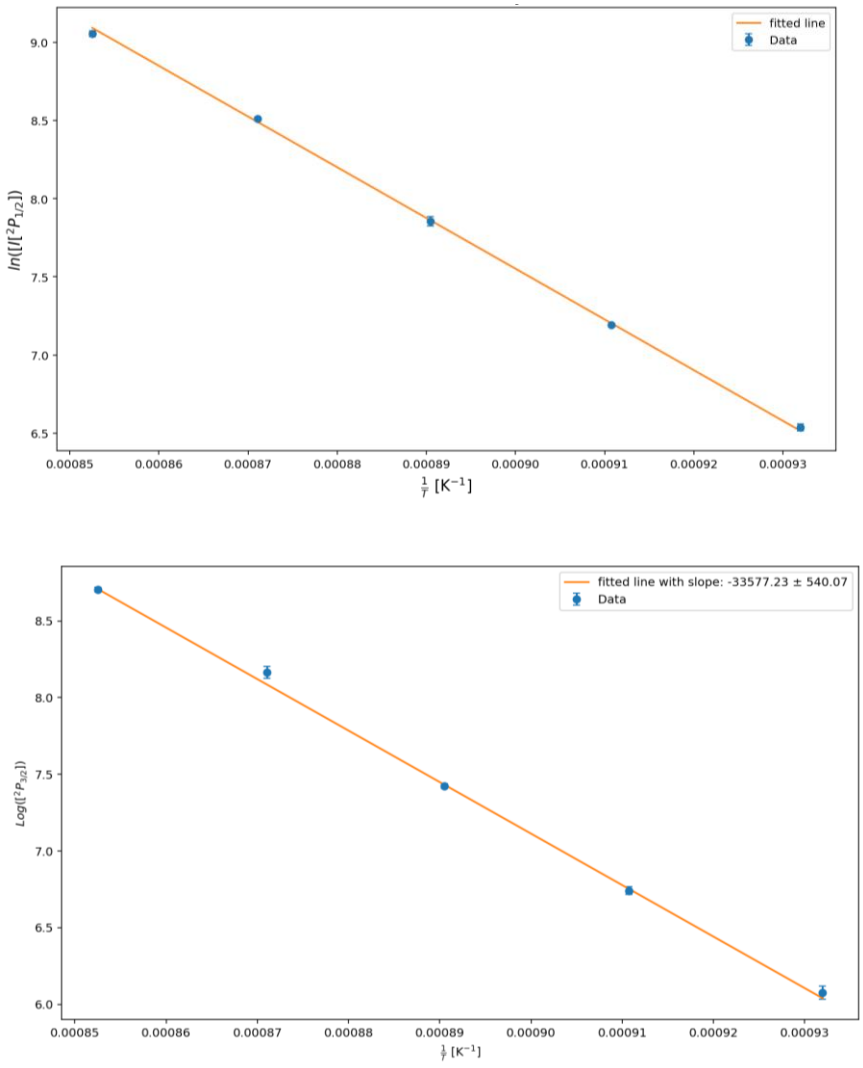

Fig. 10: Arrhenius plots used to calculate vaporization enthalpies ΔH_{vap}. The plot demonstrates ln(Signal intensity) vs. 1/T with a fitted line.

We obtain ΔH_{vap} = (270±4) kJ/mol for the ground state, and ΔH_{vap} = (279±4) kJ/mol for the first excited spin-orbit state. According to Zhang Y. et al, ΔH_{vap} = 256 kJ/mol at the boiling point (2400°C).

Secondly, we look at the population ratio as a function of temperature. The Boltzmann distribution predicted when the electronic states are in equilibrium with the liquid:

$$\frac{[^2P_{3/2}]}{[^2P_{1/2}]} = \frac{g_{3/2}}{g_{1/2}}\, e^{-\frac{\Delta E}{kT(liquid)}},\ \ \Delta E = E_{3/2} - E_{1/2},$$

where [i] is the population, g is the degeneracy, and k is the Boltzmann constant.

The LIF measured data points represent the transition intensities. To convert the intensity ratio to population ratio, we use the following formula:

$$\frac{[^2P_{3/2}]}{[^2P_{1/2}]} = \frac{I(^2P_{3/2})}{I(^2P_{1/2})}\,\frac{B_{1/2}}{B_{3/2}},$$

Where I is the measured intensity and B is the Einstein stimulated emission coefficient. The Einstein B coefficient could be calculated using the following formula:

$$B_{12} = \frac{g_2}{g_1}\,\frac{A_{21}c^3}{8\pi\, h\, \nu^3},$$

Where A is the Einstein spontaneous emission constant (easily available via the NIST atomic transition database [21]), c is the speed of light, and h is the Planck constant [22]. Then the measured population ratio becomes:

$$\frac{[^2P_{3/2}]}{[^2P_{1/2}]} = \frac{I(^2P_{3/2})}{I(^2P_{1/2})}\,(\frac{\nu_{3/2}}{\nu_{1/2}})^3\,\frac{g_{3/2}}{g_{1/2}}\,\frac{A_{1/2}}{A_{3/2}},$$

The measured and predicted population ratios are expressed graphically in figure 4.

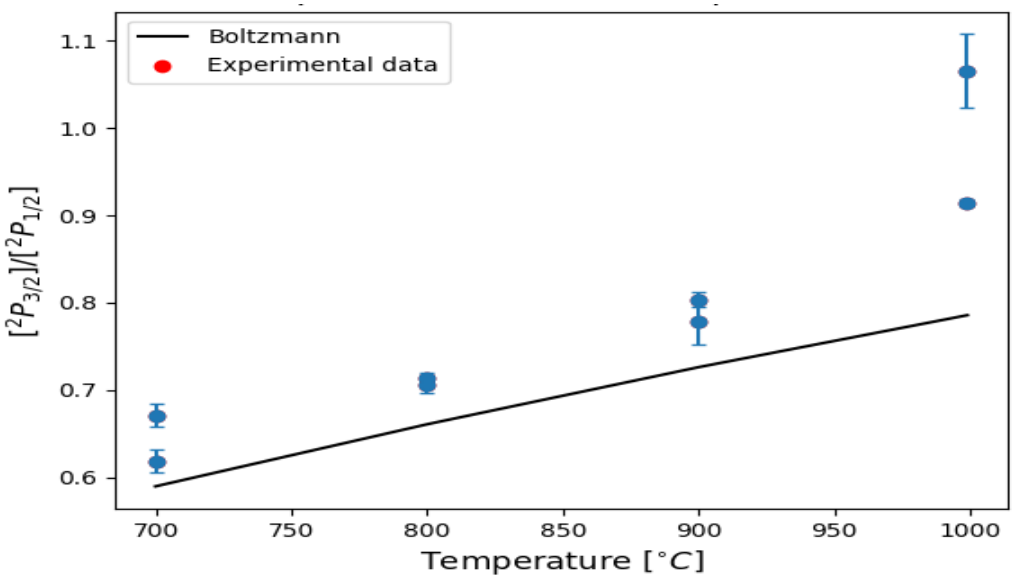

Fig. 11: Experimental population ratio vs. temperature. Each point consists of the average intensity of three scans of Ga ($^2P_{3/2}$) divided by the average intensity of three scans of Ga ($^2P_{1/2}$).

6. Discussion

We must first clarify that, even though we truly seek a flux measurement of the atoms leaving and entering the gas-liquid interface, LIF spectroscopy measures the density of the atoms in a specific energy state but not the flux. Considering the relation: flux α density*velocity, we assume that the velocity distribution is similar for the two

probed states. However, this might not be relevant to the true physical process which would open a potential area of further research.

Our results indicate that, in the range 700-900°C, the probability of incoming atoms in the gas-molten metal system bouncing off the liquid (P_b) is measurable within precision of the measurements made. However, the gallium oxide thin film and flacks forming on the top of the sample might play a role in that. Reliable data are to be collected after applying the best possible cleaning methods, including an in-vacuum mechanical scraper.

According to the detailed balance principle, for an equilibrium system of gas in contact with a liquid surface, the rate of incoming atoms is equal to the rate of atoms leaving the surface. If we imagine a screen in a distance much closer to the surface than the mean free path of the gas molecules, we can see that the one-way flux (R_{eq}) is an upper limit to the thermal desorption rate since some incident atoms on the liquid interface might bounce off and pass through the screen without being desorbed. We can identify the probability (P_s) that an incident atom "sticks" to the surface and show that the true rate of equilibrium thermal desorption (R_D) is

$$R_D = P_s\, R_{eq},$$

where P_s and R_{eq} are temperature dependent. Using the data in the previous section, we can characterize the adsorption/desorption process using P_s [4]. We found that P_b is observed to be non-zero at the temperature range of 700-900°C.

Looking at the signal dependance on temperature for each electronic state, we can determine the heat of vaporization for atoms in those states. We obtain ΔH_{vap} = (270±4) kJ/mol for the ground state, and ΔH_{vap} = (279±4) kJ/mol for the first excited spin-orbit state. Note that the energy splitting between the two states is 826 $cm^{-1} \approx 9.88\ kJ/mol$, which is consistent with the measured difference in heat of vaporization of the two states as expected.

7. Conclusion:

The results show a noticeable bouncing probability of incident gaseous Ga atoms on the liquid interface in the range (700-900°C). However, further data collection with oxide-free sample is needed for more a concrete conclusion. The heat of vaporization was measured at a relatively low temperature range - compared to the boiling point – and we obtained the values ΔH_{vap} = (270±4) kJ/mol for the ground state, and ΔH_{vap} = (279±4) kJ/mol for the first excited spin-orbit state. Further investigation of the velocity distribution of the atoms leaving the liquid metal is needed to understand he dynamics at the gas-molten metal interface since our study did investigated density but not flux.

References

[1] Zutz, Amelia Marie, "Quantum State-Resolved Collision Dynamics of Nitric Oxide at Ionic Liquid and Molten Metal Surfaces" (2017). Chemistry & Biochemistry Graduate Theses & Dissertations. 2018.

[2] Mikhail Ryazanov, David J. Nesbitt; Quantum-state-resolved studies of aqueous evaporation dynamics: NO ejection from a liquid water microjet. J. Chem. Phys. 28 January 2019; 150 (4): 044201.

[3] Zhang Y; Evans JRG; Zhang S (2011). "Corrected Values for Boiling Points and Enthalpies of Vaporization of Elements in Handbooks". J. Chem. Eng. Data. 56 (2): 328–337.

[4] John C Tully, “The dynamics of adsorption and desorption”, Surface Science, Volumes 299–300, 1994, Pages 667-677, ISSN 0039-6028.

[5] Continuum, “Operation and Maintenance Manual for the Powerlite Precision 8000 Series Laser”, 1993.

[6] Paschotta, R. "Q Switching", RP Photonics Encyclopedia, retrieved 2024-03-26.

[7] Tooley, Michael H., Electronic circuits: fundamentals and applications. (2006). Newnes. pp. 77–78. ISBN 978-0-7506-6923-8.

[8] Koechner, W., Solid-State Laser Engineering. Springer, 2006, Chapter 8, ISBN-10: 0-387-29094-X.

[9] Continuum, Operation and Maintenance Manual for the ND6000 Series Dye Laser. 1994.

[10] NC Air Awareness Program, It’s our air. 2014. https://www.deq.nc.gov/airaware/ioa/ioa1-1actair100115

[11] Mehio, Nada; Dai, Sheng; and De-en Jiang, Quantum Mechanical Basis for Kinetic Diameters of Small Gaseous Molecules. The Journal of Physical Chemistry A. 2014 118 (6), 1150-1154. DOI: 10.1021/jp412588f

[12] Atkins, P.; Paula, J., Physical Chemistry. W. H. Freeman and Company, New York, 2006. Chapter 21.

[13] Haynes, W. M.; Lide, David R.; Bruno, Thomas J., CRC Handbook of Chemistry and Physics. CRC Press, 2014. 95th Edition.

[14] Burgess, C., OPTICAL SPECTROSCOPY | Detection Devices, Encyclopedia of Analytical Science. Second Edition, 2005.

[15] Gorban, A.N., Detailed balance in micro- and macrokinetics and micro-distinguishability of macro-processes, 2014. Results in Physics 4, 142–147.

[16] Chabala, Jan M., Oxide-growth kinetics and fractal-like patterning across liquid gallium surfaces, 1992. Phys. Rev. B 46, 11346.

[17] Mondal B, Mukherjee T, Finch NW, Saha A, Gao MZ, Palmer TA, DebRoy T. Vapor Pressure versus Temperature Relations of Common Elements. Materials (Basel). 2022 Dec 21;16(1):50. doi: 10.3390/ma16010050. PMID: 36614385; PMCID: PMC9821539.

[18] Slater, J. C. (1964). "Atomic Radii in Crystals". Journal of Chemical Physics. 41 (10): 3199–3205.

[19] Kawamoto, E. H., S. Lee, Peter S. Pershan, M. Deutsch, N. Maskil, and B. M. Ocko. 1993. X-ray reflectivity study of the surface of liquid gallium. Physical Review B 47(11): 6847-6850.

[20] Carleton, K. L., Bourguignon, B., Leone, S., Desorption of a two-state system: Laser probing of gallium atom spin-orbit states from silicon (100), 1988. Surface Science 199 (1988) 447-466

[21] Kramida, A., Ralchenko, Yu., Reader, J., and NIST ASD Team (2023). NIST Atomic Spectra Database (ver. 5.11), [Online]. Available: https://physics.nist.gov/asd. National Institute of Standards and Technology, Gaithersburg, MD. DOI: https://doi.org/10.18434/T4W30F.

[22] Hilborn, R.C., Einstein coefficients, cross sections, f values, dipole moments, and all that. 2002. Revised version of Am. J. Phys. 50, 982-986 (1982). https://arxiv.org/abs/physics/0202029.